Role of the Crystal Structure in Cation Exchange Reactions Involving Colloidal Cu$_2$Se Nanocrystals

Graziella Gariano,[†] Vladimir Lesnyak,[⊥] Rosaria Brescia,[‡] Giovanni Bertoni,[†,¶] Zhiya Dang,[†] Roberto Gaspari,[†,§] Luca De Trizio,*[,†] and Liberato Manna*[,†]

[†]Nanochemistry Department, [‡]Electron Microscopy Facility, and [§]CompuNet, Istituto Italiano di Tecnologia, via Morego 30, 16163 Genova, Italy

[⊥]Physical Chemistry, TU Dresden, Bergstr. 66b, 01062 Dresden, Germany

[¶]IMEM-CNR, Parco Area delle Scienze, 37/A, 43124 Parma, Italy

Ⓢ Supporting Information

ABSTRACT: Stoichiometric Cu$_2$Se nanocrystals were synthesized in either cubic or hexagonal (metastable) crystal structures and used as the host material in cation exchange reactions with Pb^{2+} ions. Even if the final product of the exchange, in both cases, was rock-salt PbSe nanocrystals, we show here that the crystal structure of the starting nanocrystals has a strong influence on the exchange pathway. The exposure of cubic Cu$_2$Se nanocrystals to Pb^{2+} cations led to the initial formation of PbSe unselectively on the overall surface of the host nanocrystals, generating Cu$_2$Se@PbSe core@shell nanoheterostructures. The formation of such intermediates was attributed to the low diffusivity of Pb^{2+} ions inside the host lattice and to the absence of preferred entry points in cubic

Cu$_2$Se. On the other hand, in hexagonal Cu$_2$Se nanocrystals, the entrance of Pb^{2+} ions generated PbSe stripes "sandwiched" in between hexagonal Cu$_2$Se domains. These peculiar heterostructures formed as a consequence of the preferential diffusion of Pb^{2+} ions through specific (a, b) planes of the hexagonal Cu$_2$Se structure, which are characterized by almost empty octahedral sites. Our findings suggest that the morphology of the nanoheterostructures, formed upon partial cation exchange reactions, is intimately connected not only to the NC host material, but also to its crystal structure.
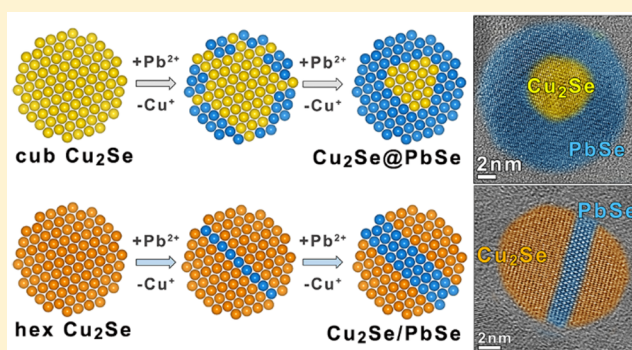
INTRODUCTION

Postsynthetic transformations of nanocrystals (NCs) have emerged as a powerful approach for the fabrication of complex nanomaterials with controlled architectures or composition.[1−5] Among them, cation exchange (CE) reactions in solution have been increasingly exploited as an efficient synthetic means for preparing nanoheterostructures (NHs) that would be inaccessible otherwise, or even metastable materials with unique composition and morphology.[6−9] Also, over the last couple of years, CE reactions have been observed to take place in the solid state when different nanostructures were heated up in the high vacuum environment of a transmission electron microscope (TEM).[10−12] The knowledge accumulated so far on CE reactions has enabled, this last year alone, the synthesis of new types of NHs, such as CdS nanowires covered by a monolayer of MoS$_2$,[13] Cu$_2$S-decorated CdS nanorods (NRs),[14] and new core@shell NC systems such as Mn$_3$O$_4$@CoMn$_2$O$_4$−Co$_x$O$_y$,[15] Ag−Zn−In-S@ZnS,[16] and SnTe@CdTe.[17−20] Moreover, the number of new NC materials that can be accessed by CE with control over the shape,[21−25] crystal structure,[26] and composition[27−34] has also increased significantly. In turn, these advanced nanostructures have found application in many

different fields such as bioimaging,[16,20,28,30,35] chemical sensing,[30] supercapacitors,[21] electro- or photocatalysis,[14,15] and spintronic or optoelectronic devices.[13,23,32]

The latest studies have emphasized how a fine-tuning of the composition, crystal structure, morphology, and thus, the properties of nanostructures synthesized by CE reactions, can be attained only when the kinetics or the mechanisms that underly a specific transformation are better understood.[6,14,16,31,34,36−41] We recently demonstrated, for example, how the valence and the coordination number of the entering cations (also called guest cations) influence the CE reaction pathways in NCs, leading to different possible NHs by partial CE.[42,43] However, from a mechanistic point of view, some aspects of CE reactions must still be investigated. For example, it is not clear yet how the ligands on the surface of host NCs exactly influence the entrance of guest cations or the release of host ions during a CE reaction.[6,8]

In this work, we have investigated how the crystal structure of a host NC material influences its CE reaction, an aspect that

has also remained not much explored to date. The system studied here involves the exchange between Cu_2Se NCs, as the host lattice, and Pb^{2+} ions as guest cations. Cu_2Se NCs were chosen as a case study material for two main reasons: (i) it is possible to synthesize Cu_2Se NCs in both cubic and hexagonal (metastable) crystal structures; (ii) copper chalcogenide NCs are a relatively well studied host material for CE reactions because Cu^+ cations can be easily replaced with harder Lewis acids (e.g., Zn^{2+}, In^{3+}, Sn^{2+}, Sn^{4+}, Ag^+, and Cd^{2+}) by employing soft Lewis bases like alkyl phosphines.[6] Reactions involving Cu_2Se NCs and Pb^{2+} ions, in comparison, are much less studied (one notable case is represented by PbSe-PbS heterostructures synthesized from Cu_2Se-Cu_2S NHs).[44−46]

The main findings of our work are the following: in the case of cubic Cu_2Se NCs, the reaction started unselectively from the surface of the NCs, gradually proceeding toward the core, and producing, as intermediate structures, $Cu_2Se@PbSe$ core@shell NHs (see Scheme 1, upper panel). This conformed to the low

Scheme 1. Cation Exchange Reaction between Either Cubic or Hexagonal Cu_2Se NCs and Pb^{2+} Cations
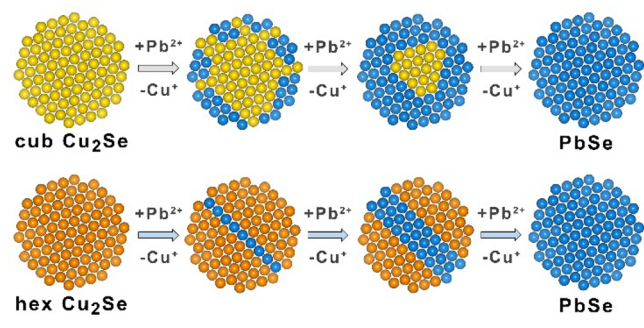
diffusivity of the Pb^{2+} ions along any crystallographic direction of the cubic Cu_2Se phase. Instead, in the case of hexagonal Cu_2Se NCs, the Pb^{2+} ions entered the host NCs through specific lattice planes (002 planes) leading to $Cu_2Se/PbSe$ striped NHs as intermediate structures (see Scheme 1, lower panel).

This peculiar behavior is rationalized by considering that, along these planes, the Pb^{2+} ions can move almost undisturbed by hopping through octahedral (Oh) sites that are almost entirely vacant, a unique feature of the metastable hexagonal Cu_2Se structure. The peculiarity of such heterostructures is that in each NC the product PbSe stripe is located in between two Cu_2Se domains. This is markedly different from CE reactions reported so far, in which the newly formed material grew by enchasing or "sandwiching" the host material.[6] The different transformation mechanisms characterizing the two cases, in turn, led to different total exchanged PbSe NC samples. Starting from cubic Cu_2Se NCs as the host material, monocrystalline defect-free rock-salt (rs) PbSe NCs were produced. On the other hand, when exposing hexagonal Cu_2Se NCs to Pb^{2+} ions, the resulting rs-PbSe NCs were also monocrystalline, but in many cases exhibited twin boundaries.

The present study highlights the importance of the crystal structure of the host lattice in nanoscale CE transformations, as this can directly influence the ion exchange pathways. In fact, our results demonstrate how the phase of starting NCs can play a fundamental role not only in accessing a specific nano-heterostructure by partial CE, but also has a profound impact

on the crystalline quality of product NCs in the case of total CE.

EXPERIMENTAL SECTION

Chemicals. Cadmium oxide (CdO, 99.5%), trioctylphosphine oxide (99%), trioctylphosphine (TOP, 97%), selenium powder (Se, 99.99%), and lead(II) acetate trihydrate ($Pb(CH_3CO_2)_2\cdot3H_2O$, 99.999%) were purchased from Strem Chemicals. Octadecylphosphonic acid (99%) was purchased from Polycarbon Industries. Copper(II) acetylacetonate ($Cu(acac)_2$, 97%), hexadecylamine (98%), tetrakis(acetonitrile)copper(I) hexafluorophosphate (99.99%), octadecene (technical grade, 90%), 1-dodecanethiol (≥98%), oleylamine (70%), tetrachloroethylene (≥99%), anhydrous chloroform, methanol, toluene, and tetrahydrofuran were purchased from Sigma-Aldrich. All chemicals were used without any further purification.

Synthesis of Cubic $Cu_{2−x}Se$ NCs. The synthesis of cubic $Cu_{2−x}Se$ NCs was adapted from the work of Li et al.[47] The copper precursor (CuCl, 99 mg) was mixed with hexadecylamine (HDA, 1 g) and octadecene (5 mL) in a three-neck flask and degassed at 130 °C for 1 h. The system was then put under N_2 flux and the temperature was set to 300 °C. The selenium precursor (3 mL of a 0.5 M solution of selenium powder dissolved in oleylamine) was injected when the reaction solution reached 300 °C. After 10 min from the injection, the flask was cooled down to room temperature, and 3 mL of chloroform was added. The NCs were washed by precipitation upon addition of ethanol followed by redispersion in toluene.

Reduction of Cubic $Cu_{2−x}Se$ into Cu_2Se NCs. The reduction of the as-synthesized cubic $Cu_{2−x}Se$ NCs was done following a procedure that we recently published.[48] $Cu(acac)_2$ (262 mg, 1 mM) was mixed with 1.5 mL of 1-dodecanethiol, 3 mL of oleylamine, and 4.5 mL of octadecene in a three-neck round-bottom flask, and the resulting solution was degassed under vacuum and vigorous stirring at 60 °C for 1 h. Then the flask was filled with nitrogen, and the temperature was raised to 120 °C to dissolve the copper precursor. Thereafter, the temperature was lowered to 100 °C, and 2.5 mL of TOP was injected followed by subsequent addition of the crude reaction mixture of $Cu_{2−x}Se$ NCs. The resulting mixture was maintained for 20 min at 100 °C, and it was subsequently cooled down to room temperature. The NCs were separated by centrifugation, dispersed in toluene, and precipitated with the addition of ethanol.

Synthesis of Hexagonal Cu_2Se NCs. Hexagonal Cu_2Se NCs were prepared by CE starting from wurtzite (wz) CdSe NCs. The latter were synthesized following the procedure reported by Carbone et al.[49] The cadmium precursor (CdO, 60 mg) was mixed with octadecylphosphonic acid (OPA, 290 mg) and trioctylphosphine oxide (TOPO, 3 g) in a three-neck flask and degassed at 130 °C for 1 h. It is important to underline here that we deliberately avoid the addition of hexylphosphonic acid in the reaction mixture as this surfactant is known to favor a rod-like morphology in wz-CdSe.[50] The flask was then filled with N_2, and the temperature was set to 300 °C, to allow the complete dissolution of the cadmium precursor. After the addition of TOP (1.9 mL), the temperature was increased to 380 °C, the value at which the selenium precursor (58 mg of selenium powder dissolved in 500 mg of TOP) was injected. The NCs were allowed to grow for 10 min. Then the flask was cooled down to room temperature, and 3 mL of toluene were added. The particles were precipitated by addition of ethanol and redispersed in toluene. The cleaning procedure was repeated twice.

The as-synthesized CdSe NCs were then transformed into Cu_2Se NCs following the CE procedure reported by Sadtler et al.[51] CdSe NCs (with a concentration of 0.005 mmol of Cd^{2+}) were dispersed in 0.2 mL of toluene in a vial. Then the copper precursor solution (0.025 mmol of tetrakis(acetonitrile)copper(I) hexafluorophosphate, dissolved in 1 mL of methanol) was added. After few seconds, the NCs were precipitated by centrifugation and, eventually, redispersed in toluene.

CE Reactions between Cu_2Se NCs and Pb^{2+} Ions. All the CE reactions were performed in a N_2-filled glovebox at room temperature.

In a typical CE reaction, a desired amount (see Table 1) of a 0.1 M methanolic stock solution of the Pb precursor ($Pb(OAc)_2 \cdot 3H_2O$) was

Table 1. Synthetic Parameters Used in CE Reactions with Pb^{2+} Ions and the Composition of the Corresponding Products

sample	Pb/Se feed ratio	reaction time	final composition
cubic Cu_2Se	40:1	48 h	$Cu_{0.11}Pb_{1.02}Se$
	1:2	30 min	$Cu_{1.18}Pb_{0.54}Se$
hexagonal Cu_2Se	40:1	overnight	$Cu_{0.07}Pb_{1.02}Se$
	1:2	30 min	$Cu_{0.92}Pb_{0.58}Se$

diluted with 0.5−1 mL of methanol and mixed with 1 mL of tetrahydrofuran, 0.5 mL of TOP, and 0.2 mL of Cu_2Se NCs in toluene (Se content = 0.025−0.03 mM). After the mixture was stirred, the resulting NCs were precipitated by centrifugation and were redispersed by addition of 1−2 mL of toluene. The NCs were further washed by addition of 2 mL of methanol to remove the excess of cation precursors and were precipitated by centrifugation. Eventually, the cleaned NCs were dispersed in toluene and stored in a N_2-filled glovebox. Note that to allow a complete CE, a large excess of Pb-precursor (Pb/Se ≈ 40) was used (2 mL of a 1.3 M methanolic stock solution).

Transmission Electron Microscopy (TEM) Characterization. Bright field TEM (BF-TEM) imaging was performed on a JEOL JEM-1011 microscope equipped with a thermionic gun operating at 100 kV accelerating voltage. For these analyses, the samples were prepared by dropping dilute suspensions of NCs onto carbon coated 200 mesh copper grids. High-resolution TEM (HRTEM) imaging, high-angle annular dark field (HAADF)-scanning TEM (STEM) imaging, and energy-dispersive X-ray spectroscopy (EDS) analyses were carried out with a JEOL JEM-2200FS microscope equipped with a Schottky emitter working at an accelerating voltage of 200 kV, a CEOS spherical aberration corrector for the objective lens, and a Bruker Quantax 400 system with a 60 mm^2 XFlash 5060 silicon drift detector (SDD). For these latter analyses, the NC suspensions were drop-cast onto carbon coated gold grids. The EDS spectra were quantified using the Cliff-Lorimer method for the Cu $K\alpha$, Se $K\alpha$, Pb $L\alpha$ peaks, and the reported STEM-EDS maps were obtained by integrating the intensities over the same peaks. In HAADF, an inner cutoff angle above 100 mrad was used to enhance the chemical contrast and to reduce possible coherent effects on the contrast due to strain or defects.

X-ray Diffraction (XRD) Measurements. The XRD analysis was performed on a PANalytical Empyrean X-ray diffractometer equipped with a 1.8 kW CuKα ceramic X-ray tube and PIXcel^{3D} 2 × 2 area detector, operating at 45 kV and 40 mA. Specimens for the XRD measurements were prepared in a glovebox by dropping a concentrated NCs solution onto a quartz zero-diffraction single crystal substrate. The diffraction patterns were collected in air at room temperature using a parallel beam geometry and symmetric reflection mode. XRD data analysis was carried out using HighScore 4.1 software from PANalytical. The Le Bail fit of the XRD pattern was performed using the Fox program.[52,53]

Elemental Analysis. The elemental analysis was carried out via inductively coupled plasma optical emission spectroscopy (ICP-OES) on a iCAP 6000 Series ICP-OES spectrometer (ThermoScientific). In a volumetric flask, each sample was dissolved in aqua regia (HCl/HNO$_3$ 3:1 (v/v)) and left overnight at room temperature to completely digest the NCs. Afterward, Milli-Q grade water (18.3 MΩ cm) was added to the sample. The solution was then filtered using a polytetrafluorethylene (PTFE) membrane filter with 0.45 μm pore size. All chemical analyses performed by ICP-OES were affected by a systematic error of about 5%.

Optical Absorption Measurements. Optical absorption measurements were carried out using a Varian Cary 5000 UV−vis-NIR spectrophotometer and 1 cm path length quartz cuvettes. A dilute dispersion of NCs in tetrachloroethylene, which ensures no interference from the solvent in NIR extinction measurements, was

prepared inside a nitrogen filled glovebox. The chemical composition of the ligand shell was characterized by an attenuated total reflectance accessory (MIRacle ATR, PIKE Technologies) coupled to a Fourier transform infrared (FTIR) spectrometer (Equinox 70 FT-IR, Bruker). The measurements on the dried samples were conducted within 4000−600 cm^{-1} range with a resolution of 4 cm^{-1} and 128 repetitive scans averaged for each spectrum.

Computational Modeling. Density functional theory (DFT) calculations were performed on bulk models of hexagonal stoichiometric Cu_2Se using the primitive unit cell and two sets of fractional coordinates as described in Table S1 of the Supporting Information (SI). We used the Perdew−Burke−Enzerhof[54] functional, ultrasoft[55] pseudopotentials for all elements, and the pwscf code.[56] Respectively, 30 and 240 Ryd were used as cutoff for the plane waves and charge density. A Monkhorst−Pack 6 × 6 × 3 mesh was used for Brillouin zone sampling. Geometry optimization was carried out up to a largest force of 0.0001 atomic units.

■ RESULTS AND DISCUSSION

Colloidal Cu_2Se NCs with either cubic or hexagonal crystal structure were synthesized with similar size and stoichiometry and used as host material for CE reactions with Pb^{2+} ions. In both cases, as it will be shown below, the starting NCs were purposely produced with an aspect ratio as close to unity as possible to minimize shape effects and to avoid the presence of high energy surface defects, which typically characterize anisotropic NCs.[6] As a matter of fact, CE reactions in NCs with a high aspect ratio, like NRs and nanoplatelets, have been shown to start at specific preferential sites such as the tips of the rods or the lateral facets of the platelets.[51,57−61]

Cubic $Cu_{2−x}Se$ NCs were synthesized, following a procedure reported by Li et al.,[47] with a cuboctahedral shape and a mean size of 10.4 ± 1.3 nm, as shown in the TEM image of Figure S1 of the SI. The crystal structure of such NCs well matched with that of cubic $Cu_{2−x}Se$ berzelianite (ICSD card no. 98−004−1140) as evidenced by our XRD analysis (see Figure 1c). The mean composition of copper selenide NCs, measured by ICP elemental analysis, was typically in the range of $Cu_{1.75}Se$ to $Cu_{1.78}Se$, evidencing a substoichiometry in copper, distinctive of this material.[24,42,47,48,62,63] Cu vacancies in copper chalcogenides are known not only to favor the diffusion of cations, boosting CE reactions, but also to offer guest cations random entry points.[48,64] To focus on the effects of the crystal structure of the host NCs in CE reactions, and to avoid the influence of other parameters, such as the presence of Cu vacancies, the cubic $Cu_{2−x}Se$ NCs were transformed to stoichiometric Cu_2Se. This was done by the incorporation of additional Cu^+ ions in a reducing environment, following a procedure recently published by us.[48] The elemental analysis confirmed that the transformed copper selenide NCs had a Cu/Se ratio around 2:1 while preserving the same size, shape and, most important, the cubic crystal structure of the starting $Cu_{2−x}Se$ NCs (see Figure 1a,c). As expected, the insertion of Cu^+ ions led to a small expansion of the lattice parameters, which increased from 5.694 Å in $Cu_{2−x}Se$ NCs to 5.746 Å in Cu_2Se ones (evidenced by the small shift of the XRD peaks toward lower 2theta angles, see Figure 1c). Another proof of the change in stoichiometry, that follows the reduction process, was given by the optical features of $Cu_{2−x}Se$ and Cu_2Se NCs: the localized surface plasmon resonance at about 1100 nm, arising from the presence of Cu vacancies in substoichiometric $Cu_{2−x}Se$ NCs, disappeared in Cu_2Se NCs (see Figure S2 of the SI).

With the aim to compare hexagonal and cubic Cu_2Se NC systems, it was of utmost importance to start from NCs having,
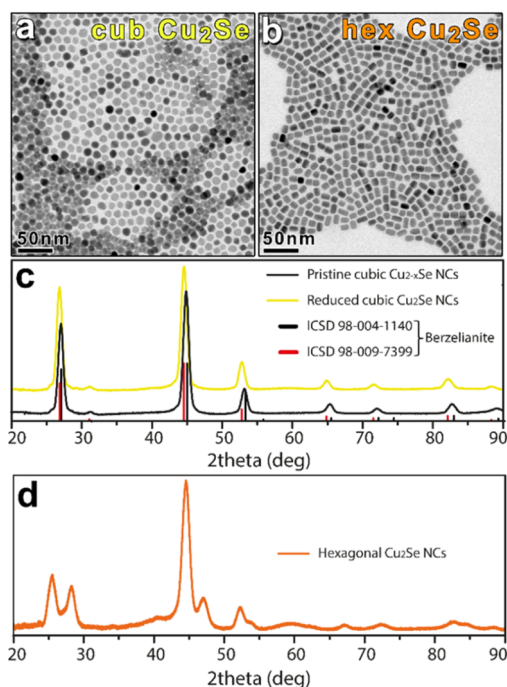
Figure 1. BF-TEM images of (a) cubic Cu_2Se and (b) hexagonal Cu_2Se NCs. (c) XRD patterns of the as-synthesized cubic $Cu_{2-x}Se$ NCs (black line) and of the reduced (yellow line) cubic Cu_2Se NCs. The corresponding bulk cubic berzelianite reflections are also shown by black bars (ICSD 98−004−1140) and red bars (ICSD 98−009−7399). (d) XRD pattern of hexagonal Cu_2Se NCs.

as mentioned above, comparable size and shape. As Cu_2Se does not crystallize in a hexagonal phase, metastable hexagonal Cu_2Se NCs could be synthesized only via CE from wz-CdSe NCs, as we reported in our previous works.[64,65] On the other hand, driven by the intrinsic anisotropy of the wurtzite structure, CdSe NCs typically tend to grow along the c axis forming rod-like structures rather than spherical NCs.[50] To overcome this potential issue, we adopted the procedure reported by Carbone et al.[49] with minor modifications (see the Experimental Section for details), which delivered nearly monodisperse wz-CdSe NCs with a size of 10.0 ± 1.2 nm and an aspect ratio of 1.18 (see Figure S3 of the SI). After the complete replacement of Cd^{2+} with Cu^+ cations, the resulting copper selenide NCs retained the size and shape of parent CdSe NCs, and they had the expected metastable "chalcocite-like" hexagonal structure, as confirmed by our XRD analysis (see Figure 1b,d, Figures S3a and S4 of the SI).[65] As assessed by ICP elemental analysis, the hexagonal Cu_2Se NCs were stoichiometric, and they did not show any localized surface plasmon resonance (see Figure S2 of the SI).

It is worth mentioning that cubic and hexagonal Cu_2Se NCs were characterized by a different ligating environment as a consequence of the diverse synthetic approaches adopted for their synthesis. More specifically, the cubic Cu_2Se NCs were passivated by HDA ligands, whereas the hexagonal Cu_2Se NCs were passivated by OPA and TOPO (see the Experimental Section and Figure S5a of the SI). In the attempt to have both NC systems passivated by the same ligands, we tried different ligand exchange procedures, however, with poor results. The exposure of the metastable hexagonal Cu_2Se NCs to HDA led to their phase transformation into a tetragonal $Cu_{1.5}Se$ phase (see Figure S5b of the SI). Conversely, the native ligands of

cubic Cu_2Se NCs could not be replaced by OPA (see Figure S5a of the SI). In any case, although the different ligand environments should affect the exchange rate of cations (and, consequently, the speed of the CE reaction), we believe that their role on dictating the pathway of CE should not be as strong at that represented by the symmetry of the lattice itself.

Both cubic and hexagonal Cu_2Se NCs were employed in CE reactions with Pb^{2+} cations at room temperature. It is worth noting that PbSe and Cu_2Se bulk materials are not miscible so that partial CE experiments should lead to heterostructures.[6−9] The exposure of cubic and hexagonal Cu_2Se NCs to an excess of Pb^{2+} ions (see the Experimental Section for details) led, in both cases, to NCs with same size and shape of the parental copper selenide NCs and a crystal structure that well matched with that of rs-PbSe clausthalite (ICSD number 98−006−3097, see Figure 2 and Figure S6 of the SI).
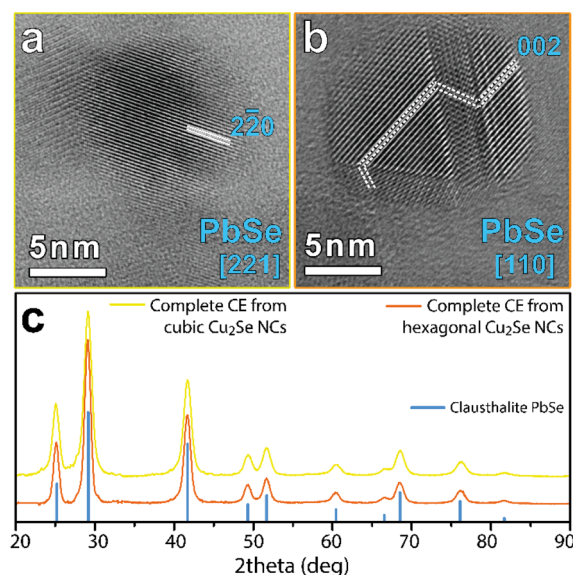
**Figure 2.** HRTEM images of PbSe NCs obtained starting from (a) cubic Cu_2Se and (b) hexagonal Cu_2Se NCs. (c) XRD patterns of the complete CE products together with the corresponding bulk reflections of cubic clausthalite PbSe (light blue bars, ICSD 98−006−3097).

The ICP elemental analysis further confirmed the presence of Pb and Se elements with a very low residual amount of Cu^+ ions (see Table 1). Both PbSe samples had similar optical features, that is, no photoluminescence and comparable absorption curves (see Figure S7 of the SI). Interestingly, while in the case of cubic Cu_2Se NCs the complete exchange, achieved using a huge excess of Pb^{2+} ions (Pb:Se feed ratio of 40:1), required 48 h, in the case of hexagonal Cu_2Se NCs, already after ~12 h almost no traces of residual copper were detected by the elemental analysis (see Table 1). Another difference in the two CE reactions emerged from the high-resolution TEM analysis of the product NCs: while PbSe NCs synthesized from cubic Cu_2Se NCs were found to be monocrystalline and defect-free (see Figure 2a), the NCs produced starting from hexagonal Cu_2Se NCs exhibited, in many cases, twin boundaries, as evidenced by Figure 2b and Figure S8 of the SI.

To understand the differences between the two CE reactions, we performed partial CE experiments to study in detail the resulting products. When Cu^+ cations of cubic Cu_2Se NCs were

partially replaced by Pb^{2+} ions, the final sample mainly consisted of $Cu_2Se@PbSe$ core@shell NHs (see Figure 3 and
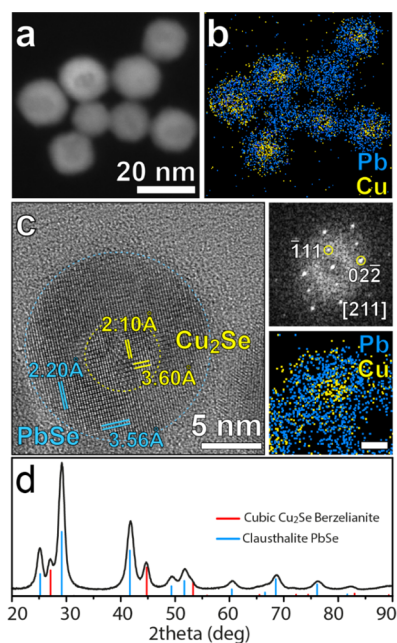
Figure 3. (a) HAADF-STEM image of a group of $Cu_2Se@PbSe$ core@shell NHs with the corresponding (b) STEM-EDS elemental map for Cu and Pb. (c) HRTEM image of a single $Cu_2Se@PbSe$ core@shell NC with the corresponding FFT (top right panel) and STEM-EDS map for Cu and Pb (bottom right panel). The scale bar in the EDS map is 5 nm. The dotted yellow and light blue lines, delimiting the cubic Cu_2Se core and the PbSe shell, are a guide for the eyes. (d) XRD pattern of the sample obtained by partial CE of cubic Cu_2Se NCs and Pb^{2+} ions. The bulk XRD reflections of cubic Cu_2Se berzelianite (ICSD 98−009−7399) and PbSe clausthalite (ICSD 98−006−3097) are also reported by red and light blue bars, respectively.

the Experimental Section for details). HAADF-STEM images of partially exchanged NCs evidenced, indeed, the presence of a brighter shell surrounding a darker core, which can be intuitively ascribed to PbSe and Cu_2Se, respectively (see Figure 3a). The HRTEM and EDS characterizations of such NHs further confirmed that the shell was made of rs-PbSe, while the core corresponded to cubic Cu_2Se (see Figure 3b,c and Figure S9 of the SI). The presence of both rs-PbSe and the berzelianite Cu_2Se phases was supported also by XRD analysis, as shown in Figure 3d.

These findings, similar to what observed in our previous work, suggest that the low diffusivity of large octahedrally coordinated Pb^{2+} ions led to the unselective formation of the PbSe domains on the whole surface of Cu_2Se NCs, favored, most likely, by the absence of preferred entry points.[43] The different PbSe nuclei that form on the surface of the starting NCs at the early stages of the exchange (see Figure S9 of the SI) eventually grow and merge (the reaction front moves toward the NC's center) forming a uniform PbSe shell and evolve into defect-free PbSe NCs. This can be rationalized by considering that clausthalite PbSe and berzelianite Cu_2Se crystal structures are both characterized by a face-centered cubic Se anion sublattice with similar lattice parameters: a_{Cu_2Se} = 5.746 Å and a_{PbSe} = 6.121 Å. The $Cu_2Se → PbSe$ transformation can be accomplished by a small expansion of

the Se sublattice (∼6% elongation of a) which, most likely, takes place without the formation of strain-induced defects.

Differently from the previous case, the exposure of hexagonal Cu_2Se NCs to a substoichiometric amount of Pb^{2+} ions (i.e., using a Pb/Se feed ratio of 1:2) led to the formation of striped $Cu_2Se/PbSe$ NHs (see Figure 4). As it was possible to observe
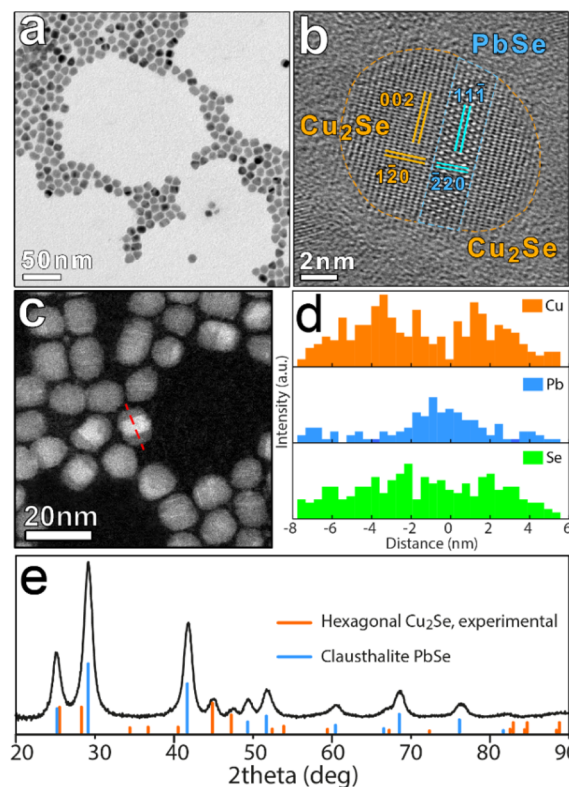
Figure 4. (a) BF-TEM image of the product NCs obtained by partial CE of hexagonal Cu_2Se NCs and Pb^{2+} ions. (b) HRTEM image of a striped hex-$Cu_2Se/PbSe$ NH. (c) HAADF-STEM image of a group of partially exchanged hexagonal Cu_2Se NCs. It is possible to notice the presence of both striped hex-$Cu_2Se/PbSe$ NHs and Cu_2Se NCs in which only few layers of PbSe formed upon CE. (d) EDS line-scan performed along the red line marked in panel c. (e) XRD pattern of the product resulting from the partial CE between hexagonal Cu_2Se NCs and Pb^{2+} ions with the corresponding bulk reflections of clausthalite PbSe (light blue bars, ICSD 98−006−3097). As a guide for the eyes, the experimental reflections measured for the starting hexagonal Cu_2Se NCs (see Figure 1d) are also reported by orange bars.

in BF-TEM images, a fraction of the resulting NCs was characterized by a striped texture with domains showing different contrast (see Figure 4a). HAADF-STEM and EDS analyses of those structures evidenced the occurrence of inner high-contrast Pb-rich regions and outer low-contrast Cu-rich domains (see Figure 4c,d). Furthermore, HRTEM images of such NHs confirmed the presence of a central PbSe domain and lateral hexagonal Cu_2Se domains, as shown in Figure 4b. XRD and ICP elemental analyses further supported these results evidencing the presence of both the hexagonal Cu_2Se and the PbSe structures, with a mean $Cu_{0.92}Pb_{0.58}Se$ composition (see Figure 4e and Table 1).

The notable finding here is that the product PbSe is "sandwiched" between the remaining hexagonal Cu_2Se domains. Except for rare cases, in all the CE reactions reported
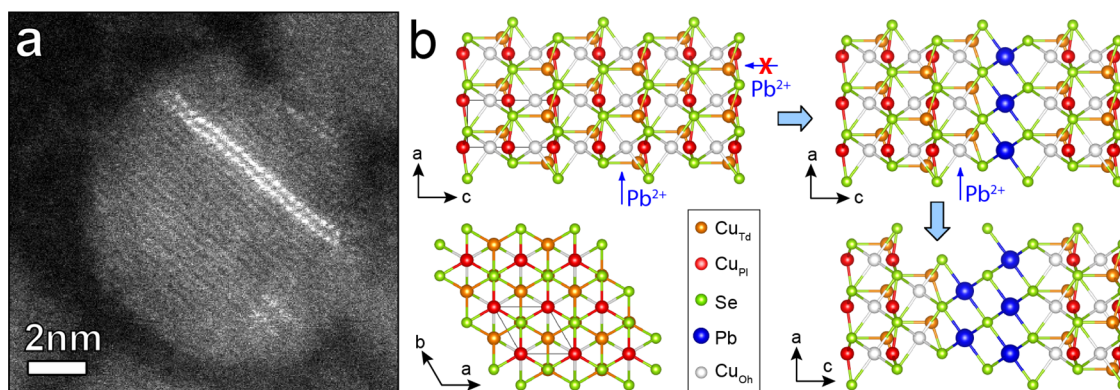
Figure 5. (a) HAADF-STEM image of a single partially exchanged hexagonal Cu_2Se NC. It is possible to notice the presence of two PbSe stripes in the middle of the NC. (b) Atomic schemes representing the hexagonal Cu_2Se structure: (upper left panel) side view and (lower left pane) top view. The hexagonal cell is indicated in black. Orange and red spheres represent Cu^+ ions in Td and Pl coordination, respectively. From the side view, it is possible to visualize the preferential a, b planes through which Pb^{2+} ions (blue spheres) can diffuse inside the host structure occupying the Oh sites, highly vacant in Cu^+ (white spheres). The insertion of lead is believed to proceed mainly in a layer-by-layer fashion as schematized (upper and lower right panels).

up to date, the formation of the product material was observed to occur either from the overall surface of the host NCs, yielding core@shell NHs, or from one surface site, forming Janus-like NHs, or from multiple surface sites, creating multidomain or striped NHs in which the host material is "sandwiched" in between the product material.[6−9] The only exceptions are represented by striped Ag_2S/CdS NRs and Cu_2S/Ag_2S nanowires.[66,67] In the first case, the CE reaction between CdS NRs and Ag^+ was observed to produce, at the early stages, small Ag_2S nuclei randomly dispersed over the NR surface, which, subsequently, coalesced forming regularly spaced Ag_2S segments.[67] The formation and the stabilization of such superlattices were attributed to the large interfacial strain between the two materials and to the consequent repulsive elastic interaction among the Ag_2S sections.[68] In the second example, the CE between Cu_2S nanowires and Ag^+ ions was observed to produce multiple Ag_2S stripes perpendicular to the elongation of the wires.[66] The generation of these peculiar NHs was proven to be driven by the presence of numerous twin boundaries in the starting Cu_2S nanowires, which acted as preferred nucleation sites for the Ag_2S phase.

Considering the different morphology of our $Cu_2Se/PbSe$ NHs compared to Ag_2S/CdS superlattices (i.e., there are no PbSe stripes "repelling" each other), and that the starting hexagonal Cu_2Se are not characterized by the presence of twin boundaries (see Figure S4 of the SI and ref 65), the formation of striped NHs observed here cannot be explained by strain- or defect-induced CE processes. Upon closer inspection of HAADF-STEM images of Pb-partially exchanged samples, we observed that, in many NCs, single or double PbSe layers formed along (a, b) planes of Cu_2Se NCs (see Figures 4c, 5a and Figure S10 of the SI). These findings indicate that Pb^{2+} ions had preferential entry points through which they access and diffuse into the host Cu_2Se NCs. To better sift this hypothesis, we performed an accurate refinement of the metastable hexagonal Cu_2Se structure, which, up to now, has not been analyzed in detail. Our Le Bail fit of the experimental XRD pattern (see Figure S11 of the SI) revealed that the hexagonal Cu_2Se phase can be accurately described with a P63/mc symmetry (as in wurtzite), in which copper cations occupy not only the tetrahedral (Td) site (with Wyckoff position 2b), but also a quasi-planar (Pl) site at position 2a (see Figure 5b

and Figure S12 of the SI). On the other hand, the octahedral (Oh) sites are essentially empty (see Figure 5b, white spheres and Figure S12 of the SI). The stability of this structure was also confirmed by our DFT calculations. Furthermore, these calculations confirmed that the Cu_2Se P63/mc structure with occupied Oh sites is unstable: the copper ions in Oh sites relax upon shifting to the near Pl sites (see Table S1 of the SI). These findings evidence a preferential site occupancy in the hexagonal Cu_2Se structure, which provides unusual wide diffusion planes for guest ions that are not found in any known cubic copper selenide.[24,69] These preferred sites are stabilized by the rigid hexagonal close-packed $Se^{2−}$ anion sublattice of wz-CdSe that is preserved in hexagonal Cu_2Se (see Figure 5b and Figure S13 of the SI). The insertion of Pb^{2+} ions in wz-CdSe NCs (and in general in hexagonal Cd-based chalcogenide NCs) has been reported to start from the (001) or the (00−1) facets.[51,60,70] By comparing wz-CdSe and the present hexagonal Cu_2Se structures, it is clear that in the latter no diffusion channels along the c-direction are available for Pb^{2+} ions, most likely as a consequence of the presence of the second Cu^+ ion in Pl coordination (see Figure 5b and Figure S4 of the SI). On the other hand, the hexagonal Cu_2Se structure, differently from wz-CdSe, is characterized by preferential (a, b) diffusion planes for Pb^{2+} ions, in which the latter can adopt the desired Oh coordination, confirming what observed in HAADF-STEM images. When two layers of PbSe form inside the hexagonal Cu_2Se, they adopt the cubic structure, which can be achieved by a minor shift of the surrounding Se anions. The shifted Se atoms further block the diffusion of guest ions along the c direction by occupying the empty channels in the wurtzite type structure (i.e., 2a site). Bearing this in mind, the formation of twinned PbSe NCs in complete CE from hexagonal Cu_2Se NCs can be, thus, explained as follows: when two separate PbSe stripes form in a single hexagonal Cu_2Se NC and grow, due to the ABC stacking of the cubic structure in the PbSe stripe, there is only a $1/3$ probability that a matching is observed at the interface between the two domains.

■ CONCLUSION

In conclusion, we have shown that cubic and hexagonal (metastable) Cu_2Se NCs can undergo CE with Pb^{2+} ions at room temperature. In both systems, the final product of the

exchange is rs-PbSe NCs. We demonstrated that the crystal structure of the starting NCs material can dictate the CE pathway. In cubic Cu_2Se NCs, PbSe nucleates randomly on the overall surface of the host material, generating $Cu_2Se@PbSe$ core@shell NHs as intermediates. This exchange trend, already observed in other CE transformations, can be explained taking into account the low diffusivity of Pb^{2+} ions coupled with the absence of preferred entry points in cubic Cu_2Se. On the other hand, in hexagonal Cu_2Se NCs, Pb^{2+} ions could diffuse and replace host cations along defined (a, b) planes of the host material, generating PbSe stripes "sandwiched" in between Cu_2Se domains. This peculiar CE process, not observed in any other known system, was attributed to the hexagonal metastable Cu_2Se structure, which presents preferred entry points to the guest ions. Indeed, the hexagonal Cu_2Se is characterized by (002) planes with almost empty Oh sites, which Pb^{2+} ions can access to diffuse inside the host material. Our findings, thus, suggest that the crystal structure of host NCs is an important parameter that should be taken into account when performing CE reactions. More precisely, we observed that both the crystalline quality and morphology of the nanostructures obtained by CE are sensitive to the phase of starting NCs.

■ ASSOCIATED CONTENT

Ⓢ Supporting Information

The Supporting Information is available free of charge on the ACS Publications website at DOI: 10.1021/jacs.7b03706.

> Low resolution TEM images of $Cu_{2-x}Se$, CdSe, and PbSe NCs; histograms of particle size distribution; absorption curves of $Cu_{2-x}Se$ and Cu_2Se NCs; XRD pattern of CdSe NCs; HRTEM of hexagonal Cu_2Se, PbSe, $Cu_2Se@PbSe$, and $Cu_2Se/PbSe$ NCs; atomic scheme of wurzite CdSe and hexagonal Cu_2Se; Le Bail fit; DFT calculations (PDF)

■ AUTHOR INFORMATION

Corresponding Authors
*luca.detrizio@iit.it
*liberato.manna@iit.it

ORCID Ⓘ
Vladimir Lesnyak: 0000-0002-2480-8755
Giovanni Bertoni: 0000-0001-6424-9102
Luca De Trizio: 0000-0002-1514-6358
Liberato Manna: 0000-0003-4386-7985

Notes
The authors declare no competing financial interest.

■ ACKNOWLEDGMENTS

■ REFERENCES

(1) Vasquez, Y.; Henkes, A. E.; Chris Bauer, J.; Schaak, R. E. *J. Solid State Chem.* **2008**, *181*, 1509−1523.

(2) Buck, M. R.; Schaak, R. E. *Angew. Chem., Int. Ed.* **2013**, *52*, 6154−6178.

(3) Xiaodong, C.; Harald, F. *Soft Matter Nanotechnology: From Structure to Function*; Wiley-VCH Verlag GmbH & Co. KGaA: Weinheim, 2015.

(4) Moon, G. D.; Ko, S.; Min, Y.; Zeng, J.; Xia, Y.; Jeong, U. *Nano Today* **2011**, *6*, 186−203.

(5) Fayette, M.; Robinson, R. D. *J. Mater. Chem. A* **2014**, *2*, 5965−5978.

(6) De Trizio, L.; Manna, L. *Chem. Rev.* **2016**, *116*, 10852−10887.

(7) Son, D. H.; Hughes, S. M.; Yin, Y.; Paul Alivisatos, A. *Science* **2004**, *306*, 1009−1012.

(8) Rivest, J. B.; Jain, P. K. *Chem. Soc. Rev.* **2013**, *42*, 89−96.

(9) Gupta, S.; Kershaw, S. V.; Rogach, A. L. *Adv. Mater.* **2013**, *25*, 6923−6944.

(10) Casu, A.; Genovese, A.; Manna, L.; Longo, P.; Buha, J.; Botton, G. A.; Lazar, S.; Kahaly, M. U.; Schwingenschloegl, U.; Prato, M.; Li, H.; Ghosh, S.; Palazon, F.; De Donato, F.; Lentijo Mozo, S.; Zuddas, E.; Falqui, A. *ACS Nano* **2016**, *10*, 2406−2414.

(11) Buha, J.; Manna, L. *Chem. Mater.* **2017**, *29*, 1419−1429.

(12) Chen, Y. H.; Huang, C. W.; Yeh, P. H.; Chen, J. Y.; Lin, T. Y.; Chang, C. F.; Wu, W. W. *Nanoscale* **2016**, *8*, 17039−17043.

(13) Tan, C.-S.; Lu, Y.-J.; Chen, C.-C.; Liu, P.-H.; Gwo, S.; Guo, G.-Y.; Chen, L.-J. *J. Phys. Chem. C* **2016**, *120*, 23055−23060.

(14) Sun, Z.; Liu, X.; Yue, Q.; Jia, H.; Du, P. *ChemCatChem* **2016**, *8*, 157−162.

(15) Luo, Z.; Irtem, E.; Ibáñez, M.; Nafria, R.; Martí-Sánchez, S.; Genç, A.; de la Mata, M.; Liu, Y.; Cadavid, D.; Llorca, J.; Arbiol, J.; Andreu, T.; Morante, J. R.; Cabot, A. *ACS Appl. Mater. Interfaces* **2016**, *8*, 17435−17444.

(16) Song, J.; Ma, C.; Zhang, W.; Li, X.; Zhang, W.; Wu, R.; Cheng, X.; Ali, A.; Yang, M.; Zhu, L.; Xia, R.; Xu, X. *ACS Appl. Mater. Interfaces* **2016**, *8*, 24826−24836.

(17) Jang, Y.; Yanover, D.; Čapek, R. K.; Shapiro, A.; Grumbach, N.; Kauffmann, Y.; Sashchiuk, A.; Lifshitz, E. *J. Phys. Chem. Lett.* **2016**, *7*, 2602−2609.

(18) Lee, S.; Baek, S.; Park, J. P.; Park, J. H.; Hwang, D. Y.; Kwak, S. K.; Kim, S.-W. *Chem. Mater.* **2016**, *28*, 3337−3344.

(19) Wu, W.-Y.; Chakrabortty, S.; Guchhait, A.; Wong, G. Y. Z.; Dalapati, G. K.; Lin, M.; Chan, Y. *Chem. Mater.* **2016**, *28*, 9132−9138.

(20) Teitelboim, A.; Oron, D. *ACS Nano* **2016**, *10*, 446−452.

(21) Tang, Y.; Chen, S.; Mu, S.; Chen, T.; Qiao, Y.; Yu, S.; Gao, F. *ACS Appl. Mater. Interfaces* **2016**, *8*, 9721−9732.

(22) Ramasamy, P.; Kim, M.; Ra, H.-S.; Kim, J.; Lee, J.-S. *Nanoscale* **2016**, *8*, 7906−7913.

(23) Choi, J. Y.; Lee, S. J.; Seo, W. S.; Song, H. *CrystEngComm* **2016**, *18*, 6069−6075.

(24) White, S. L.; Banerjee, P.; Jain, P. K. *Nat. Commun.* **2017**, *8*, 14514.

(25) Zhang, C.; Xia, Y.; Zhang, Z.; Huang, Z.; Lian, L.; Miao, X.; Zhang, D.; Beard, M. C.; Zhang, J. *Chem. Mater.* **2017**, *29*, 3615−3622.

(26) Wang, Y.; Morozov, Y. V.; Zhukovskyi, M.; Chatterjee, R.; Draguta, S.; Tongying, P.; Bryant, B.; Rouvimov, S.; Kuno, M. *ACS Energy Lett.* **2016**, *1*, 175−181.

(27) Roudebush, J. H.; Ross, K. A.; Cava, R. J. *Dalton Trans.* **2016**, *45*, 8783−8789.

(28) Gabka, G.; Bujak, P.; Kotwica, K.; Ostrowski, A.; Lisowski, W.; Sobczak, J. W.; Pron, A. *Phys. Chem. Chem. Phys.* **2017**, *19*, 1217−1228.

(29) Doh, H.; Hwang, S.; Kim, S. *Chem. Mater.* **2016**, *28*, 8123−8127.

(30) Han, S.; Qin, X.; An, Z.; Zhu, Y.; Liang, L.; Han, Y.; Huang, W.; Liu, X. *Nat. Commun.* **2016**, *7*, 13059.

(31) Enright, M. J.; Sarsito, H.; Cossairt, B. M. *Chem. Mater.* **2017**, *29*, 666−672.

(32) Saha, A.; Makkar, M.; Shetty, A.; Gahlot, K.; Pavan, A. R.; Viswanatha, R. *Nanoscale* **2017**, *9*, 2806−2813.

(33) Xu, Y.-Z.; Yuan, C.-Z.; Chen, X.-P. *RSC Adv.* **2016**, *6*, 106832−106836.

(34) Zheng, Z.; Sun, Y.-Y.; Xie, W.; Zhao, J.; Zhang, S. *J. Phys. Chem. C* **2016**, *120*, 27085−27090.

(35) Zhao, Z.; Chi, X.; Yang, L.; Yang, R.; Ren, B. W.; Zhu, X.; Zhang, P.; Gao, J. *Chem. Mater.* **2016**, *28*, 3497−3506.

(36) Dzhagan, V.; Kempken, B.; Valakh, M.; Parisi, J.; Kolny-Olesiak, J.; Zahn, D. R. T. *Appl. Surf. Sci.* **2017**, *395*, 24−28.

(37) Meir, N.; Martín-García, B.; Moreels, I.; Oron, D. *Chem. Mater.* **2016**, *28*, 7872−7877.

(38) White, S. L.; Banerjee, P.; Chakraborty, I.; Jain, P. K. *Chem. Mater.* **2016**, *28*, 8391−8398.

(39) Chakraborty, P.; Jin, Y.; Barrows, C. J.; Dunham, S. T.; Gamelin, D. R. *J. Am. Chem. Soc.* **2016**, *138*, 12885−12893.

(40) Fan, Z.; Lin, L.-C.; Buijs, W.; Vlugt, T. J. H.; van Huis, M. A. *Nat. Commun.* **2016**, *7*, 11503.

(41) Kershaw, S. V.; Abdelazim, N. M.; Zhao, Y.; Susha, A. S.; Zhovtiuk, O.; Teoh, W. Y.; Rogach, A. L. *Chem. Mater.* **2017**, *29*, 2756−2768.

(42) De Trizio, L.; Li, H.; Casu, A.; Genovese, A.; Sathya, A.; Messina, G. C.; Manna, L. *J. Am. Chem. Soc.* **2014**, *136*, 16277−16284.

(43) Tu, R.; Xie, Y.; Bertoni, G.; Lak, A.; Gaspari, R.; Rapallo, A.; Cavalli, A.; Trizio, L. D.; Manna, L. *J. Am. Chem. Soc.* **2016**, *138*, 7082−7090.

(44) Mishra, N.; Mukherjee, B.; Xing, G.; Chakrabortty, S.; Guchhait, A.; Lim, J. Y. *Nanoscale* **2016**, *8*, 14203−14212.

(45) Jain, P. K.; Amirav, L.; Aloni, S.; Alivisatos, A. P. *J. Am. Chem. Soc.* **2010**, *132*, 9997−9999.

(46) Bouet, C.; Laufer, D.; Mahler, B.; Nadal, B.; Heuclin, H.; Pedetti, S.; Patriarche, G.; Dubertret, B. *Chem. Mater.* **2014**, *26*, 3002−3008.

(47) Li, W.; Zamani, R.; Ibáñez, M.; Cadavid, D.; Shavel, A.; Morante, J. R.; Arbiol, J.; Cabot, A. *J. Am. Chem. Soc.* **2013**, *135*, 4664−4667.

(48) Lesnyak, V.; Brescia, R.; Messina, G. C.; Manna, L. *J. Am. Chem. Soc.* **2015**, *137*, 9315−9323.

(49) Carbone, L.; Nobile, C.; De Giorgi, M.; Sala, F. D.; Morello, G.; Pompa, P.; Hytch, M.; Snoeck, E.; Fiore, A.; Franchini, I. R.; Nadasan, M.; Silvestre, A. F.; Chiodo, L.; Kudera, S.; Cingolani, R.; Krahne, R.; Manna, L. *Nano Lett.* **2007**, *7*, 2942−2950.

(50) Alivisatos, A. P.; Peng, X.; Manna, L.; Yang, W.; Wickham, J.; Scher, E.; Kadavanich, A. *Nature* **2000**, *404*, 59−61.

(51) Sadtler, B.; Demchenko, D. O.; Zheng, H.; Hughes, S. M.; Merkle, M. G.; Dahmen, U.; Wang, L.-W.; Alivisatos, A. P. *J. Am. Chem. Soc.* **2009**, *131*, 5285−5293.

(52) Le Bail, A. *J. Solid State Chem.* **1989**, *83*, 267−271.

(53) Favre-Nicolin, V.; Cerny, R. *J. Appl. Crystallogr.* **2002**, *35*, 734−743.

(54) Perdew, J. P.; Burke, K.; Ernzerhof, M. *Phys. Rev. Lett.* **1996**, *77*, 3865−3868.

(55) Vanderbilt, D. *Phys. Rev. B: Condens. Matter Mater. Phys.* **1990**, *41*, 7892−7895.

(56) Giannozzi, P.; Baroni, S.; Bonini, N.; Calandra, M.; Car, R.; Cavazzoni, C.; Ceresoli, D.; Chiarotti, G. L.; Cococcioni, M.; Dabo, I.; Dal Corso, A.; de Gironcoli, S.; Fabris, S.; Fratesi, G.; Gebauer, R.; Gerstmann, U.; Gougoussis, C.; Kokalj, A.; Lazzeri, M.; Martin-Samos, L.; Marzari, N.; Mauri, F.; Mazzarello, R.; Paolini, S.; Pasquarello, A.; Paulatto, L.; Sbraccia, C.; Scandolo, S.; Sclauzero, G.; Seitsonen, A. P.; Smogunov, A.; Umari, P.; Wentzcovitch, R. M. *J. Phys.: Condens. Matter* **2009**, *21*, 395502−395502.

(57) Wark, S. E.; Hsia, C.-H.; Son, D. H. *J. Am. Chem. Soc.* **2008**, *130*, 9550−9555.

(58) Jeong, S.; Han, J. H.; Jang, J.-t.; Seo, J.-w.; Kim, J.-G.; Cheon, J. *J. Am. Chem. Soc.* **2011**, *133*, 14500−14503.

(59) Mu, L.; Wang, F.; Sadtler, B.; Loomis, R. A.; Buhro, W. E. *ACS Nano* **2015**, *9*, 7419−7428.

(60) Lee, D.; Kim, W. D.; Lee, S.; Bae, W. K.; Lee, S.; Lee, D. C. *Chem. Mater.* **2015**, *27*, 5295−5304.

(61) Luther, J. M.; Zheng, H.; Sadtler, B.; Alivisatos, A. P. *J. Am. Chem. Soc.* **2009**, *131*, 16851−16857.

(62) Dorfs, D.; Härtling, T.; Miszta, K.; Bigall, N. C.; Kim, M. R.; Genovese, A.; Falqui, A.; Povia, M.; Manna, L. *J. Am. Chem. Soc.* **2011**, *133*, 11175−11180.

(63) Luther, J. M.; Jain, P. K.; Ewers, T.; Alivisatos, A. P. *Nat. Mater.* **2011**, *10*, 361−366.

(64) Miszta, K.; Gariano, G.; Brescia, R.; Marras, S.; De Donato, F.; Ghosh, S.; De Trizio, L.; Manna, L. *J. Am. Chem. Soc.* **2015**, *137*, 12195−12198.

(65) Li, H.; Zanella, M.; Genovese, A.; Povia, M.; Falqui, A.; Giannini, C.; Manna, L. *Nano Lett.* **2011**, *11*, 4964−4970.

(66) Tan, C.-S.; Hsiao, C.-H.; Wang, S.-C.; Liu, P.-H.; Lu, M.-Y.; Huang, M. H.; Ouyang, H.; Chen, L.-J. *ACS Nano* **2014**, *8*, 9422−9426.

(67) Robinson, R. D.; Sadtler, B.; Demchenko, D. O.; Erdonmez, C. K.; Wang, L.-W.; Alivisatos, A. P. *Science* **2007**, *317*, 355−358.

(68) Demchenko, D. O.; Robinson, R. D.; Sadtler, B.; Erdonmez, C. K.; Alivisatos, A. P.; Wang, L.-W. *ACS Nano* **2008**, *2*, 627−636.

(69) Danilkin, S. A.; Skomorokhov, A. N.; Hoser, A.; Fuess, H.; Rajevac, V.; Bickulova, N. N. *J. Alloys Compd.* **2003**, *361*, 57−61.

(70) Kriegel, I.; Wisnet, A.; Srimath Kandada, A. R.; Scotognella, F.; Tassone, F.; Scheu, C.; Zhang, H.; Govorov, A. O.; Rodriguez-Fernandez, J.; Feldmann, J. *J. Mater. Chem. C* **2014**, *2*, 3189−3198.